RSC Advances

PAPER

View Article Online
View Journal | View Issue

Cite this: *RSC Adv.*, 2020, **10**, 10309

Synthesis of Fe_3O_4 nanocomposites for efficient separation of ultra-small oil droplets from hexadecane–water emulsions†

Tianwen Mi, Yuxuan Cai, Qing Wang, Nuzahat Habibul, Xiaoli Ma, Zhi Su and Wei Wu *

Received 3rd February 2020
Accepted 4th March 2020

DOI: 10.1039/d0ra01044h

rsc.li/rsc-advances

Eco-friendliness and low cost are critical when investigating new oil–water separation agents with high separation efficiencies for the treatment of emulsified oily wastewater in industrial applications, including crude oil exploitation. Treatment methods specifically suited to wastewater containing ultra-small oil droplets are lacking and urgently required. This study investigated the one-pot synthesis of humic acid and polydimethyldiallylammonium chloride coated Fe_3O_4 nanoparticles. A low dosage of the nanoparticles (375 μg mL^{-1}) exhibited excellent separation efficiency (nearly 100%) and reusability when applied to hexadecane–water emulsions containing ultra-small droplets (200–300 nm). Electrostatic interactions and the strong interfacial activity of the nanoparticles played essential roles in achieving oil–water separation. This study provided an efficient extraction material synthesized by a facile and cheap method for separating ultra-small oil droplets from emulsions.

Introduction

The demand for oil resources has increased substantially in recent years, which has led to a rise in global oil production. Oily wastewater generated from crude oil exploitation poses a significant environmental and ecological threat. However, traditional methods for disposing of emulsified oily wastewater, such as gravity separation,[1] flotation,[2] electro-coalescence,[3] and membrane filtration methods,[4] have various limitations including low efficiency, high energy usage, secondary pollution generation, and high costs. Currently, the most commonly used demulsification methods applied in industry require the use of flocculating agents, acids, alkalis, salts, and chemical demulsifiers.[5] However, most of these agents are used in large quantities and cannot be recovered after demulsification, which may result in secondary pollution and resource wastage. Hence, finding an effective demulsifier for treating emulsified oily wastewater is an urgent concern.

The large surface areas and magnetic recyclability of magnetic nanoparticles (MNPs) has led to their widespread use as adsorbent materials. Oily sewage treatment using MNPs has attracted extensive interest in recent years. Peng *et al.* reported increased interfacial activity of MNPs by grafting ethyl cellulose to the surface of Fe_3O_4 nanoparticles for the oil–water separation of heavy oil and diluted bitumen emulsions.[6,7] Several amphiphilic chemical and biological materials have since been used to modify MNPs for improving demulsification efficiency.[8–11] The negative surface potential of oil-in-water emulsions and positively charged MNPs with amino groups contribute to preferable oil–water separation performance. For example, Fe_3O_4 MNPs were synthesized by coprecipitation method, and an SiO_2 layer and (3-aminopropyl)triethoxysilane were deposited on the MNPs surface using a two-step method. The resulting amphiphilic demulsifier exhibited excellent oil–water separation performance in emulsions with oil droplet sizes ranging 0.4 to 10 μm.[12–14] Lü *et al.* produced Fe_3O_4 MNPs using a solvothermal method, followed by aminopropyl functionalization using a modified Stöber method. The surface of the material was further modified with aldehyde and grafted with chitosan (CS). This four-step method produced CS-grafted MNPs with good oil–water separation performance in emulsions with oil droplet sizes below 6 μm.[15] These previous studies indicated that amphiphilic modification of MNPs is critical for the separation of emulsified oil from wastewater, while most of the amino group-modified magnetic demulsifier synthesis methods were tedious, time consuming and not environmentally friendly because of the use of harmful organic solvents.[15–17] Furthermore, most previous studies investigated the separation of oil droplets larger than 400 nm. Ultra-small emulsified oil droplets are too stable to be separated and a simple, environmentally friendly, economic and effective amine-functionalized amphiphilic magnetic material has not yet been developed for treating emulsified oil wastewater containing ultra-small oil droplets.

College of Chemistry and Chemical Engineering, Xinjiang Normal University, Urumqi, 830054, China

† Electronic supplementary information (ESI) available. See DOI: 10.1039/d0ra01044h

Humic acid (HA) is a major component of natural organic matter and possesses a rich variety of functional groups, including carboxyls, hydroxyls, carbonyls and phenolic hydroxyls. These groups have a high affinity for minerals due to their capacity to interact *via* anion exchange, ligand exchange, hydrophobic interactions, cation bridging and entropic effects.[18,19] Humic acid-coated Fe_3O_4 nanoparticles (Fe_3O_4@HA NPs) are widely used in wastewater treatment specifically for the efficient removal of various materials, such as heavy metals,[20] toxic inorganic arsenic species,[21] the radionuclide Eu(III),[22] and anionic phosphates.[23] However, these nanoparticles are rarely used to separate oil from water in emulsified oily wastewater,[24,25] due to the low separation efficiency attributed to both negative surface charge of Fe_3O_4@HA NPs and emulsified droplets. To improve their adsorption capabilities the surface potential of Fe_3O_4@HA NPs needs to be changed from negative to positive through further surface modifications.

Poly dimethyldiallylammonium chloride (PDDA) is an economical, safe, and non-toxic cationic polyelectrolyte commonly used as a flocculant in wastewater treatment. In previous studies, PDDA was used to change the hydrophilic properties of membranes that were subsequently applied to oil–water separation in emulsions.[26,27] In addition, because of the substantial quaternary ammonium groups in PDDA, PDDA-coated Fe_3O_4 (Fe_3O_4@PDDA) NPs can absorb aqueous organic phosphonates *via* electrostatic attraction.[28] Therefore, PDDA can be used to modify the surface potential and hydrophilic characteristics of Fe_3O_4@HA NPs.

This study aimed to synthesize PDDA-coated Fe_3O_4@HA NPs (Fe_3O_4@HA@PDDA NPs) using a one-pot reaction. This magnetic demulsifier was characterized by powder X-ray diffraction (XRD), Fourier-transform infrared spectroscopy (FT-IR), transmission electron microscopy (TEM), scanning electron microscopy (SEM), zeta potential measurement and magnetization curve measurement. In comparison with Fe_3O_4@HA NPs, a low concentration of the Fe_3O_4@HA@PDDA NPs effectively separated oil and water in a hexadecane–water emulsion containing ultra-small droplets. The separation mechanism of the MNPs has been presented in detail.

Experimental section

Materials

Iron(III) chloride hexahydrate ($FeCl_3 \cdot 6H_2O$), ferrous sulfate tetrahydrate ($FeSO_4 \cdot 7H_2O$), and ammonia solution ($NH_3 \cdot H_2O$) were purchased from Tianjin Zhiyuan Chemical Reagent Co., Ltd. Humic acid sodium salt ($C_9H_8Na_2O_4$) and PDDA were purchased from Aladdin Chemistry (Shanghai, China). Hexadecane was purchased from Sigma-Aldrich. All reagents were of analytical grade and used without further purification. Distilled water was used for preparation and rinsing.

Synthesis of Fe_3O_4@HA and Fe_3O_4@HA@PDDA NPs

HA-coated Fe_3O_4 MNPs were synthesized *via* a chemical co-precipitation method.[20] First, 2.780 g of $FeSO_4 \cdot 7H_2O$ and 5.405 g of $FeCl_3 \cdot 6H_2O$ ($n(Fe^{3+}) : n(Fe^{2+}) = 2 : 1$), were dissolved in 100 mL of distilled water, pumped by a vacuum, and heated to 90 °C. Next, 10 mL of ammonium hydroxide (25%) solution and 0.77 g HA dissolved in 50 mL of water were rapidly added to the reaction system. The mixture was stirred with a magnetic mixer at 90 °C for 30 min and then cooled to 25 °C. Finally, the black precipitate was collected by centrifugation, washed with water, and dried in a vacuum oven at 65 °C.

After the synthesized Fe_3O_4@HA particles suspension cooled to room temperature, 25 mL of 10% PDDA solution was rapidly added and stirred for 2 h. The Fe_3O_4@HA@PDDA NPs were collected using centrifugation and dried in a vacuum oven at 65 °C. The synthesized Fe_3O_4@HA and Fe_3O_4@HA@PDDA NPs were then used to separate oil and water emulsions.

Preparation of emulsions

Hexadecane (400 μL) and water (20 mL) were premixed with an ultrasonic cell disrupter (JY92-2D, Ningbo Xinzhi Biological Technology Co., Ltd.) for 1 min. The mixture was then stirred (500 rpm) for 15 min at 25 ± 3 °C, and subsequently sonicated for 10 min in an ultrasonic cleaner (300 W, 40 kHz) at 25 ± 3 °C to obtain a hexadecane–water emulsion. Particle size and zeta potential measurements were conducted on 100-fold diluted emulsion samples. The particle size in the emulsion was found to be approximately 140–340 nm (Fig. S4 in the ESI†), no obvious change the size of the oil droplets was observed by DLS analysis within 18 hours.[29] The zeta potential was between approximately −20 and −30 mV. This is due to the adsorption of hydroxide ions and deprotonated fatty acid impurity in 99% pure hexadecane on the surface of oil droplets.[30–33]

Oil–water separation tests

To evaluate their oil–water separation capability, the synthesized Fe_3O_4@HA and Fe_3O_4@HA@PDDA NPs (125–750 μg mL^{-1}) were added to 20 mL of freshly prepared emulsion in a glass bottle, then the mixtures were shaken in an oscillator (Shanghai Precision Instrument Co., Ltd.) at 240 cycles min^{-1} for 180 min. The absorbance of the emulsions at the wavelength of 225 nm were recorded by UV-vis spectrophotometry (TU-1901 Beijing Purkinje General Instrument Co., Ltd.) after external magnetic separation. The oil concentrations in the separated emulsion were obtained from the standard curve (Fig. S6 in the ESI†). The oil–water separation efficiency can be calculated using the equation below:

$$E_S = \frac{C_0 - C_e}{C_0} \times 100\%$$

where E_S (%) is the oil–water separation efficiency, C_0 (mg L^{-1}) is the initial oil content of the emulsion and C_e (mg L^{-1}) is the oil concentration of the emulsion after the addition of MNPs.

Recycling test

After undergoing the oil–water separation test, the MNPs were collected using a hand magnet, washed with water and ethanol, and vacuum-dried at 65 °C for 2 h. The MNPs were subsequently reused in the next cycle of the oil–water separation test. The recycling procedure was performed for nine cycles.

Characterization

Crystalline phase identification of the Fe_3O_4@HA and Fe_3O_4@HA@PDDA NPs was conducted using XRD (Bruker D2, Germany) with Cu Kα radiation. FT-IR spectra were acquired at room temperature in the range of 400–4000 cm^{-1} using a Tensor 27 spectrometer (Bruker, Germany) *via* the KBr pellet method. The morphology of the MNPs was characterized using transmission electron microscopy (JEM-2010FEF, Japan), and scanning electron microscopy (JSM-7610F PLUS, Japan). The size distribution and surface zeta potential measurements were done using a Zetasizer Nano ZS90 instrument (Malvern Instruments Ltd., UK) at 25 °C where the laser wavelength was 633 nm and the measurement angle was 90°. The particle size and potential of each material were tested three times. The magnetic behavior of the particles was observed using vibrating-sample magnetometry (PPMS-9, Quantum Design, USA) at room temperature.

Results and discussion

Characterization of MNPs

XRD experiments were used to investigate the crystal structures of the synthesized Fe_3O_4@HA and Fe_3O_4@HA@PDDA NPs. As shown in Fig. 1, diffraction peaks were observed at 29.8, 35.2, 43.2, 57.0 and 62.8° were assigned to the (220), (311), (400), (511), and (440) lattice planes, respectively. Overall, these results indicate a cubic spinel magnetite structure in both types of NPs and suggested that the HA and PDDA coatings prevented oxidation of the MNPs.

FT-IR spectra of the Fe_3O_4@HA, PDDA, and Fe_3O_4@HA@PDDA samples are shown in Fig. 2. The absorption peak at approximately 590 cm^{-1} in curves (a) and (c) can be assigned to the Fe–O vibration of the MNPs. The peaks at 1570 and 3410 cm^{-1} are attributed to the C=O stretching[34] and –OH stretching vibrations,[35] respectively, indicating that the MNPs underwent successful modification by HA. The FTIR spectrum of PDDA (curve b) includes adsorption bands at around 1458, 1630, 2930, and 3270 cm^{-1}; these are characteristic of the C–H asymmetrical deformation vibration in N–CH_3,[36] C=C stretching,[37] CH_n, and –NH vibrations, respectively. These main characteristic peaks are also observed in the spectrum of the Fe_3O_4@HA@PDDA MNPs (curve c), which confirms that PDDA modified the surface of the Fe_3O_4@HA particles.

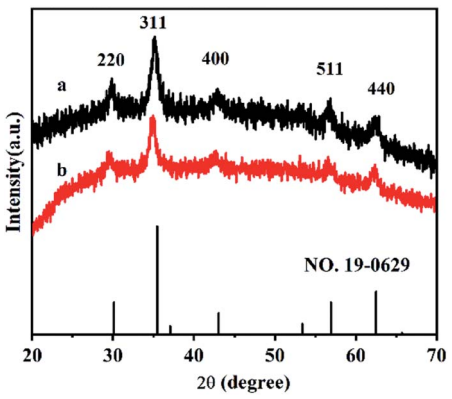

Fig. 1 XRD results. Fe_3O_4@HA@PDDA NPs (a) and Fe_3O_4@HA NPs (b) diffraction patterns.

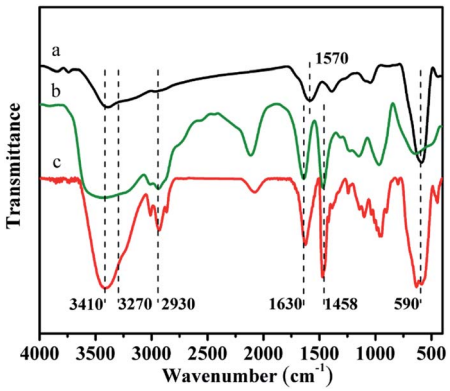

Fig. 2 FT-IR spectroscopy results for Fe_3O_4@HA NPs (a), PDDA (b), and Fe_3O_4@HA@PDDA NPs (c).

TEM and SEM images were used to evaluate the morphology and structure of MNPs. The TEM image (Fig. 3A) illustrates that the Fe_3O_4@HA NPs are monodisperse and the particle size is nanoscale, indicating the HA act as a surfactant in the process of synthesis. PDDA modification caused slight agglomeration of the Fe_3O_4@HA@PDDA NPs because a single PDDA molecule was capable of bridging multiple NPs.[38] The SEM image (Fig. 3C) further proves that the Fe_3O_4@HA@PDDA NPs retain the particle shape of their precursor Fe_3O_4@HA NPs.

Dynamic light scattering (DLS) analysis (Fig. 4) revealed that the hydrodynamic diameter of the Fe_3O_4@HA NPs was 30.6 (±12.4) nm, which increased to 105.0 (±15.8) nm after PDDA modification. The polydispersity index (PDI) values of Fe_3O_4@HA and Fe_3O_4@HA@PDDA NPs were found to be 0.119 (±0.004) and 0.203 (±0.005), respectively. These results indicate that the dispersion of the MNPs decreased upon them being modified by PDDA and that the particle size increased concomitantly, which is consistent with the TEM results.

The zeta potential of the Fe_3O_4@HA NPs was found to be −31.8 (±1.1) mV. This is a result of the large number of carboxyl and phenolic hydroxyl groups on the surface of HA. After coating with PDDA, the zeta potential changed to 28.9 (±0.9) mV, an effect attributed to the amino groups of PDDA. This result also confirms that the Fe_3O_4@HA NPs were coated with PDDA.

Fig. 5 shows the magnetization curves of the MNPs. The saturation magnetizations (M_S) of Fe_3O_4@HA and Fe_3O_4@HA@PDDA NPs were 62.4 and 51.8 emu g^{-1}, respectively. No obvious remanence or coercivity were observed, indicating that both materials are superparamagnetic. Compared with bare Fe_3O_4 (79.6 emu g^{-1}),[20] the M_S value of the MNPs decreased to a certain extent, which can be attributed to the non-magnetic HA and PDDA surface coatings. Nonetheless, despite this reduction in M_S, the magnetic response of Fe_3O_4@HA@PDDA can still prove adequate for magnetic separation.[39]

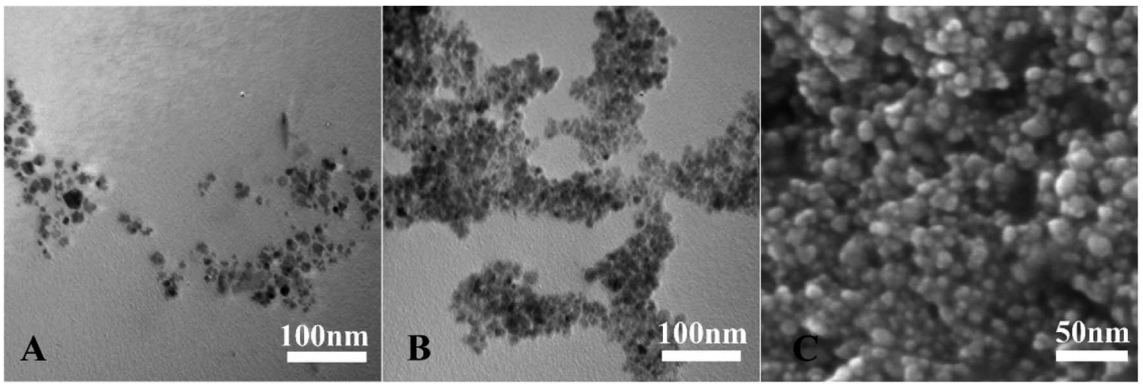

Fig. 3 Electron microscopy results. TEM images of (A) Fe_3O_4@HA NPs and (B) Fe_3O_4@HA@PDDA NPs. (C) SEM image of Fe_3O_4@HA@PDDA NPs.

Oil–water separation performance

The oil–water separation performances of the Fe_3O_4@HA and Fe_3O_4@HA@PDDA NPs within 180 min were investigated under different concentrations; the relationship between shaking time and E_S is shown in Fig. S5 in the ESI.† As can be seen from Fig. 6, E_S increases with the MNP concentration. When the concentration of Fe_3O_4@HA@PDDA is approximately 375 μg mL^{-1}, E_S is almost 100%, whereas with Fe_3O_4@HA a maximum E_S of 55.6% was achieved at a concentration of 625 μg mL^{-1}. The comparison of the E_S between Fe_3O_4@HA@PDDA and other magnetic demulsifiers in the literatures is summarized in Table 1. It was found that most of the demulsifiers[12–17,40,41] with amino group show excellent demulsification performance up to 90%,

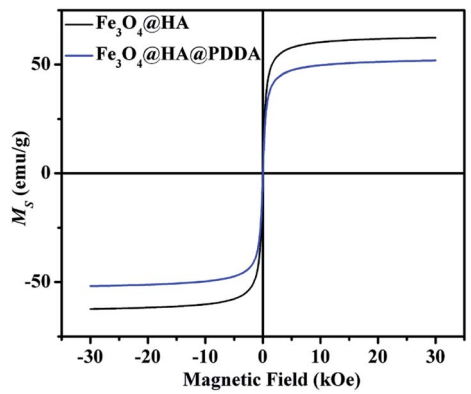

Fig. 5 Magnetization curves of Fe_3O_4@HA and Fe_3O_4@HA@PDDA NPs.

while Fe_3O_4@HA@PDDA NPs have higher oil–water separation efficiency with the least dosage except for quaternized chitosan (QC)-grafted MNPs.[16,17] In addition, Fe_3O_4@HA@PDDA NPs show higher oil–water separation efficiency for ultra-small particle emulsions (the average size of oil droplet is 247 ± 35 nm). Although oleic acid functionalized magnetic nanoparticles

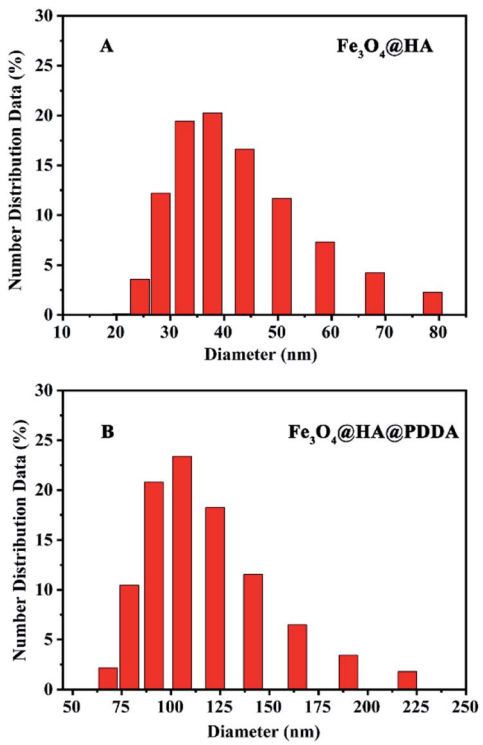

Fig. 4 Particle size analysis results. (A) Fe_3O_4@HA NPs and (B) Fe_3O_4@HA@PDDA NPs particle size distributions.

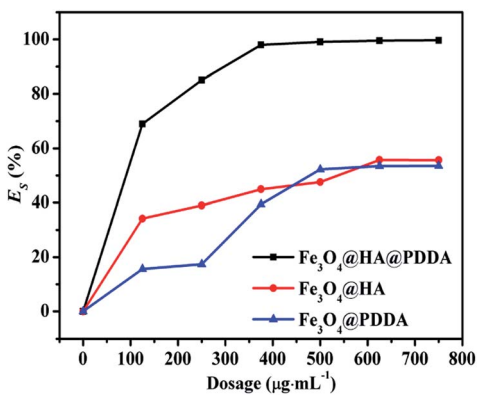

Fig. 6 Effect of magnetic nanoparticle concentration on their efficiency for separating an oil–water emulsion.

Table 1 Comparison of the demulsification efficiency between Fe_3O_4@HA@PDDA NPs and other magnetic demulsifiers (under neutral condition)[a]

Demulsifier	Dosage (mg L^{-1})	E (%)	Oil-in-water emulsion size (nm)	Emulsion concentration	Ref.
APTES-MNPs	438	99.9	200–10 000	0.25 wt%	14
EP@APTES–Fe_3O_4	500	99.9	—	1 wt%	40
Fe_3O_4@SiO_2–APTES	748	100	500	0.2 wt%	13
APTES-MNPs	800	99.7	402.3 ± 165.7	5 wt%	12
Fe_3O_4@SiO_2–QC	19	95.0	—	0.2 wt%	16
Fe_3O_4@SiO_2@APTES–QC	34	98.0	—	0.2 wt%	17
Fe_3O_4@APFS–G–CS	500	90.0	—	0.2 wt%	15
Fe_3O_4@OA	30×10^3	98.0	262	10 wt%	42
Fe_3O_4@OA	100×10^3	97.0	76	10 wt%	43
Fe_3O_4@HA@PDDA	375	100	200–300	2 wt%	This work

[a] E: oil–water separation efficiency; CS: chitosan; APFS: aminopropyl-functionalized silica; EP: expanded perlite; APTES: 3-aminopropyl triethoxysilane; MWCNTs: multi-wall carbon nanotubes; QC: quaternized chitosan.

possess 98.0% demulsification rate for the crude oil-in-water nanoemulsions with particles sized around 76 nm, the demulsifier dosage is 100×10^3 mg L^{-1},[42] which is much more than the Fe_3O_4@HA@PDDA NPs. The Fe_3O_4@HA@PDDA NPs present the advantages of high oil–water separation efficiency in ultra-small particle emulsions at a low dosage.

There are the two driving forces by which MNPs efficiently separate oil and water from an emulsion of ultra-small particles. On one hand, the Fe_3O_4@HA@PDDA NPs are driven to be adsorbed on the surface of the oil droplets in the emulsion *via* electrostatic attraction between the emulsion and the Fe_3O_4@HA@PDDA NPs. Hence, the E_S value of the Fe_3O_4@HA@PDDA NPs was significantly higher than that of Fe_3O_4@HA. Base on this, positively charged Fe_3O_4@PDDA NPs (Synthesis and Characterization in the ESI†) should also display good separation efficiencies for oil–water emulsion with ultra-small particles. However, the E_S value of Fe_3O_4@PDDA NPs is only 53.5%. To explore the reason for this unexpectedly low E_S value, the zeta potential and particle sizes of the emulsion were measured after the oil–water separation experiment. The zeta potential of the emulsion changed from −28.3 (±1.3) to −4.14 (±0.1) mV and from 247 (±19) to 335 (±9) nm, respectively. These changes indicated that the interaction between PDDA and Fe_3O_4 was weak and the oil–water separation experiment caused separation. Some of the separated PDDA absorbed onto the surface of the oil droplets which neutralized the surface potential of emulsion and increased the size. The low E_S value illustrated the poor separation performance of single PDDA due to the absence of magnetic separation. HA acted as a bridge on the surface of the Fe_3O_4 NPs to maintain a close link between PDDA and Fe_3O_4. On the other hand, interface activity also played an important role in efficient emulsion separation. The Fe_3O_4@HA@PDDA NPs exhibited an improved interface activity attributed to the abundance of hydrophobic aromatic rings and alkyl chains.

The recyclability of the Fe_3O_4@HA@PDDA nanoparticles was investigated over nine cycles, as shown in Fig. 7. After five cycles, no distinct change in E_S is observed, and the gradual decline in efficiency after six cycles is attributed to the loss of materials.

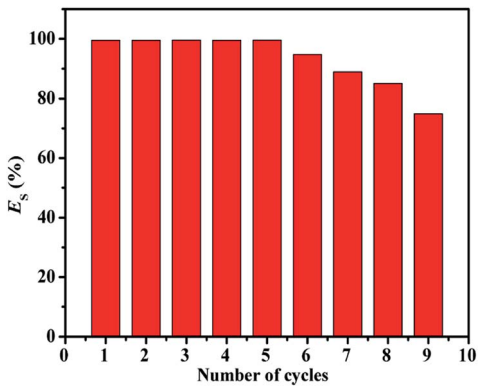

Fig. 7 Efficiency of Fe_3O_4@HA@PDDA MNPs for separating an oil–water emulsion at each of a nine-cycle sequence.

Conclusions

Positively charged Fe_3O_4@HA@PDDA NPs were synthesized using a simple one-pot synthesis process that was environmentally friendly, cost effective and produced no secondary pollution. The MNPs were used to separate oil and water in hexadecane–water emulsions containing ultra-small droplets. An oil–water separation efficiency of nearly 100% was achieved at low concentration of Fe_3O_4@HA@PDDA NPs, which is an advantage over previously reported oil–water demulsifers. The MNPs were easily regenerated and reused to minimize secondary pollution. The excellent performance was attributed to electrostatic interaction and strong interfacial activity between the Fe_3O_4@HA@PDDA NPs and the emulsified oil droplets. The MNPs were easy to synthesize and offer a high oil and water separation efficiency, which is promising for the broad application of this treatment to emulsified oil wastewater.

Conflicts of interest

There are no conflicts to declare.

Acknowledgements

This work was supported by the National Natural Science Foundation of China (NNSFC) [grant number 21763025]; the University Research Program and "Introduction of 100 Young PhDs" of Xinjiang Uygur Autonomous Region [grant numbers XJEDU2017S027, BS2016005]; and the "13th Five-Year Plan" for Key Discipline Chemistry, Xinjiang Normal University.

References

1 Z. Yu, F. F. Yun, Z. Gong, Q. Yao, S. Dou, K. Liu, L. Jiang and X. Wang, *J. Mater. Chem. A*, 2017, **5**, 10821–10826.
2 A. A. Al-Shamrani, A. James and H. Xiao, *Water Res.*, 2002, **36**, 1503–1512.
3 C. R. Vigo and W. D. Ristenpart, *Langmuir*, 2010, **26**, 10703–10707.
4 T. Rajasekhar, M. Trinadh, P. V. Babu, A. V. S. Sainath and A. V. R. Reddy, *J. Membr. Sci.*, 2015, **481**, 82–93.
5 K. Peng, Y. Xiong, L. Lu, J. Liu and X. Huang, *ACS Sustainable Chem. Eng.*, 2018, **6**, 9682–9690.
6 J. Peng, Q. Liu, Z. Xu and J. Masliyah, *Adv. Funct. Mater.*, 2012, **22**, 1732–1740.
7 J. Peng, Q. Liu, Z. Xu and J. Masliyah, *Energy Fuels*, 2012, **26**, 2705–2710.
8 N. Ali, B. Zhang, H. Zhang, W. Li, W. Zaman, L. Tian and Q. Zhang, *Fuel*, 2015, **141**, 258–267.
9 Y. Chen, X. Lin, N. Liu, Y. Cao, F. Lu, L. Xu and L. Feng, *ChemPhysChem*, 2015, **16**, 595–600.
10 T. Lü, D. Qi, D. Zhang, K. Fu, Y. Li and H. Zhao, *J. Cleaner Prod.*, 2020, **255**, 120293, DOI: 10.1016/j.jclepro.2020.120293.
11 X. Huang, Y. Xiong, L. Lu, J. Liu and K. Peng, *Energy Fuels*, 2017, **31**, 3295–3304.
12 Q. Wang, M. C. Puerto, S. Warudkar, J. Buehler and S. L. Biswal, *Environ. Sci.: Water Res. Technol.*, 2018, **4**, 1553–1563.
13 T. Lü, S. Zhang, D. Qi, D. Zhang, G. F. Vance and H. Zhao, *Appl. Surf. Sci.*, 2017, **396**, 1604–1612.
14 S. Ko, E. S. Kim, S. Park, H. Daigle, T. E. Milner, C. Huh, M. V. Bennetzen and G. A. Geremia, *J. Nanopart. Res.*, 2017, **19**, 132–146.
15 T. Lü, Y. Chen, D. Qi, Z. Cao, D. Zhang and H. Zhao, *J. Alloys Compd.*, 2017, **696**, 1205–1212.
16 T. Lü, S. Zhang, D. Qi, D. Zhang and H. Zhao, *J. Colloid Interface Sci.*, 2018, **518**, 76–83.
17 S. Zhang, T. Lü, D. Qi, Z. Cao, D. Zhang and H. Zhao, *Mater. Lett.*, 2017, **191**, 128–131.
18 E. Illés and E. Tombcácz, *J. Colloid Interface Sci.*, 2006, **295**, 115–123.
19 E. Illés and E. Tombácz, *Colloids Surf., A*, 2003, **230**, 99–109.
20 J. Liu, Z. Zhao, G. Jiang and C. Ren, *Environ. Sci. Technol.*, 2008, **42**, 6949–6954.
21 M. Rashid, G. E. Sterbinsky, M. Á. G. Pinilla, Y. Cai and K. E. O'Shea, *J. Phys. Chem. C*, 2018, **122**, 13540–13547.
22 S. Yang, P. Zong, X. Ren, Q. Wang and X. Wang, *ACS Appl. Mater. Interfaces*, 2012, **4**, 6891–6900.
23 M. Rashid, N. T. Price, M. A. Gracia Pinilla and K. E. O'Shea, *Water Res.*, 2017, **123**, 353–360.
24 S. Li, C. Wang, H. Jia, H. Liu and X. Fan, CN 102423696, National Intellectual Property of the People's Republic of China, 2011.
25 H. Jia, L. Wang and C. Wang, CN 103693170A, National Intellectual Property of the People's Republic of China, 2014.
26 J. Yang, Z. Zhang, X. Xu, X. Zhu, X. Men and X. Zhou, *J. Mater. Chem.*, 2012, **22**, 2834–2837.
27 H. Yoon, S. H. Na, J. Y. Choi, S. S. Latthe, M. T. Swihart, S. S. Al-Deyab and S. S. Yoon, *Langmuir*, 2014, **30**, 11761–11769.
28 J. Chen, Y. Ju and H. Chen, *NANO*, 2019, **14**, 1950019–1950033.
29 Y. Sang, F. Yang, S. Chen, H. Xu, S. Zhang, Q. Yuan and W. Gan, *J. Chem. Phys.*, 2015, **142**, 224704–224710.
30 J. K. Beattie and A. M. Djerdjev, *Angew. Chem., Int. Ed.*, 2004, **43**, 3568–3571.
31 K. Roger and B. Cabane, *Angew. Chem., Int. Ed.*, 2012, **51**, 5625–5628.
32 J. K. Beattie and A. Gray-Weale, *Angew. Chem., Int. Ed.*, 2012, **51**, 12941–12942.
33 H. Fang, W. Wu, Y. Sang, S. Chen, X. Zhu, L. Zhang, Y. Niu and W. Gan, *RSC Adv.*, 2015, **5**, 23578–23585.
34 B. Zhang, R. Hu, D. Sun, T. Wu and Y. Li, *J. Chem. Eng. Data*, 2018, **63**, 4689–4702.
35 L. Guo, Q.-D. An, Z. Y. Xiao, S. R. Zhai and L. Cui, *ACS Sustainable Chem. Eng.*, 2019, **7**, 9237–9248.
36 S. Wang, D. Yu and L. Dai, *J. Am. Chem. Soc.*, 2011, **133**, 5182–5185.
37 K. Liu, J. Zhang, G. Yang, C. Wang and J. J. Zhu, *Electrochem. Commun.*, 2010, **12**, 402–405.
38 S. P. Yeap and S. Y. Tia, *Chem. Eng. Res. Des.*, 2019, **142**, 53–61.
39 R. Wo, Q. L. Li, C. Zhu, Y. Zhang, G. F. Qiao, K. Y. Lei, P. Du and W. Jiang, *J. Chem. Eng. Data*, 2019, **64**, 2455–2463.
40 H. Xu, W. Jia, S. Ren and J. Wang, *Chem. Eng. J.*, 2018, **337**, 10–18.
41 H. Xu, W. Jia, S. Ren and J. Wang, *Carbon*, 2019, **145**, 229–239.
42 J. Liang, H. Li, J. Yan and W. Hou, *Energy Fuels*, 2014, **28**, 6172–6178.
43 J. Liang, N. Du, S. Song and W. Hou, *Colloids Surf., A*, 2015, **466**, 197–202.

